

Selective adsorption of Carbon Dioxide from Mixed Vapors by Blockage of Methane in Graphene Nanoribbons

Hind Aljaddani · Silvina M. Gatica*

Received: date / Accepted: date

Abstract We study numerically the adsorption of a mixture of CO₂ and CH₄ on a graphite substrate covered by graphene nanoribbons (NRs). The NRs are flat and parallel to the graphite surface, at a variable distance ranging from 6 Å to 14 Å. We show that the NRs-graphite substrate acts as an effective filter for CO₂. Our study is based on Molecular Dynamics (MD) simulations. Methane is considered a spherical molecule, and carbon dioxide is represented as a linear rigid body. Graphite is modeled as a continuous material, while the NRs are approached atomistically. We observe that when the NRs are placed 6 Å above the graphite surface, methane is blocked out, while CO₂ molecules can diffuse and be collected in between the NRs and the graphite surface. Consequently, the selectivity of CO₂ is extremely high. We also observe that the initial rate of adsorption of CO₂ is much higher than CH₄. Overall we show that the filter can be optimized by controlling the gap between NRs and the NRs-graphite separation.

Keywords gas separation · graphene nanoribbons · carbon dioxide · methane · adsorption

1 Introduction

Separating CO₂ from CH₄ is critical in industrial applications, transportation, and usage of methane [1]. Researchers have intensively investigated the adsorption

of CO₂/CH₄ mixtures on several materials like MOFs, mesoporous carbon, activated carbon, silicalite, C₁₈₆ schwarzite, and nanoporous carbon experimentally or theoretically [1, 2, 3, 4, 5, 6, 7, 8, 9].

Gas separation by adsorption can be accomplished by three physical mechanisms: equilibria, kinetics, and steric effects. Equilibrium mechanisms rely on the strength of attraction between gas molecules and the substrate, while kinetic mechanisms involve the differences in the adsorption and transport rates of gas on and through the substrate [3]. Steric mechanisms, on the other hand, depend on the incompatibility between the size or shape of the adsorbate gas molecules and the pores of the substrate. For instance, since CO₂ is typically found in a mixture with gases of similar size but different shapes (as CH₄ and N₂), steric separation may be feasible. Also, the force of some substrates is stronger to CO₂ than methane. For example, in this study, we found that the energy of interaction of CO₂ with graphite is 35% stronger than CH₄ with graphite. As a result, the equilibrium mechanism may also present an adequate strategy.

The ability of a substrate to separate gases by adsorption is measured by the selectivity. In a binary mixture of components i and j , the selectivity is defined as,

$$\Sigma(i/j) = \frac{x_i/x_j}{y_i/y_j}, \quad (1)$$

where x_i and y_i are the molar concentration of species i in the adsorbed phase and the vapor phase respectively. A high value of $\Sigma(i/j)$ indicates that the fraction of species i in the adsorbed phase is large compared to the fraction in the vapor phase, meaning that i is favorably adsorbed

In most studies of separation of CO₂/CH₄ at room temperature, the selectivities reported are smaller than

H. Aljaddani
Department of Physics and Astronomy, Howard University,
2355 Sixth St NW, Washington, DC 20059, USA
E-mail: hind.aljaddani@howard.edu

S. Gatica
Department of Physics and Astronomy, Howard University,
2355 Sixth St NW, Washington, DC 20059, USA
E-mail: sgatica@howard.edu

12. One of the highest selectivities found has been achieved by the group of Palmer et al. [8]. They investigated different types of nanoporous carbons to separate CO_2/CH_4 mixtures at ambient temperature and pressure up to 10 MPa using Grand Canonical Monte Carlo (GCMC) simulations. They found that in the carbon slit pores, the selectivity reaches 12.1 for a mixture with 25% CH_4 and at a pressure of 3 MPa. In a mix with 50% CH_4 and pressure 4 MPa, the selectivity is 11, whereas in a mixture with 75% CH_4 and pressure 6 MPa, the selectivity is 9.2.

Heuchel et al. [4] obtained $\Sigma(\text{CO}_2/\text{CH}_4)$ experimentally and theoretically on activated carbon A35/4 at 293 K. They found selectivities in the range from 2.8 to 8.9 for various concentrations and pressures. Chen et al. [10], studied the CO_2/CH_4 selectivity in a MOF-505@GO composite finding a value of 8.6 at 298 K and 100 kPa. In a recent article, Szczęśniak et al. [11] reported CO_2/CH_4 selectivity of 6.3 and 5.8 in the Cu-BTC MOF and Cu-BTC/GO10 respectively, at 298 K and 1 bar. Wang et al. [12] investigated CO_2/CH_4 separation in a penta-graphene (PG) nanosheet. They found that the selectivity is high when an electric field of 0.040 a.u. is applied. The effect of the electric field is to change the adsorbed CO_2 from physisorption to chemisorption while not affecting the methane adsorption.

Other groups found more modest values for selectivity. Bastin et al. [1] examined a microporous MOF (MOF-508b) for the separation and removal of CO_2 from binary CO_2/CH_4 , CO_2/N_2 , and ternary $\text{CO}_2/\text{CH}_4/\text{N}_2$ mixtures by fixed-bed adsorption at temperatures 303 K, 323 K, and 343 K. At 303 K for binary or ternary mixtures, the adsorption isotherms indicate that MOF-508b is moderately efficient for the removal of CO_2 . They reported that $\Sigma(\text{CO}_2/\text{CH}_4)$ and $\Sigma(\text{CO}_2/\text{N}_2)$ are in the range from 3 to 6 while decreasing with increasing temperature.

Liu et al. [5] investigated the adsorption and the selectivity of CO_2 from CO_2/CH_4 , CO_2/N_2 gas mixtures in oxygen-containing functionalized graphitic slit pores at a temperature of 298 K and pressures up to 300 bar using GCMC simulations. In their results, $\Sigma(\text{CO}_2/\text{CH}_4)$ was in the range from 2 to 5.

Babarao et al. [2], predicted the value of $\Sigma(\text{CO}_2/\text{CH}_4)$ at room temperature in three different adsorbents: silicalite, C_{168} schwarzite, and IRMOF-1. By using GCMC, they found that the selectivity of CO_2/CH_4 is in the range from 2.0 to 3.2, 2.0 to 2.6, and 3.0 to 5.0 for IRMOF-1, silicalite, and the C_{168} schwarzite, respectively. Peng et al. [9] investigated $\Sigma(\text{CO}_2/\text{CH}_4)$ on ordered mesoporous carbon CMK-1 using GCMC at $T=308$ K and for different pressures and concentrations.

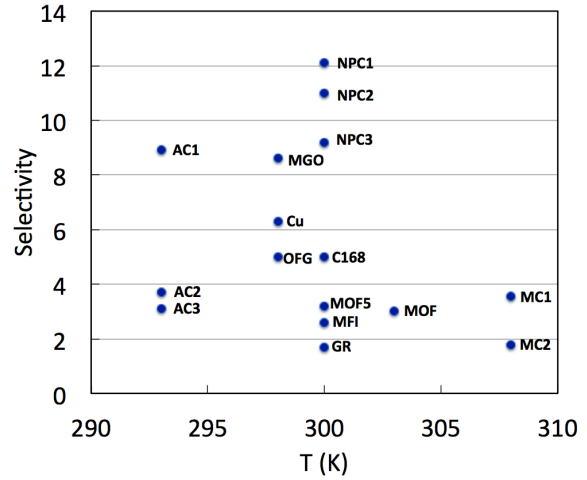


Fig. 1 Selectivity for CO_2/CH_4 near room temperature using different substrates: C_{168} , MOF5 and MFI from Ref. [2]; MOF-508b (MOF) [1]; Activated Carbon at concentrations of CO_2 90% (AC1), 50% (AC2), and 20% (AC3), respectively[4]; Oxygen-containing functionalized graphitic slit pores (OFG) [5]; graphite (GR), from this work; nanoporous carbon at 25% concentration of CH_4 and pressure 3 MPa (NPC1), 50% - 4 MPa (NPC2), and 75%- 6MPa (NPC3) [8]; mesoporous carbon CMK-1 at 20% concentration of CO_2 and pressure 7.0 MPa (MC1), and 50%-4.0 MPa (MC2) [9]; MOF-505@GO at 100kPa (MGO) [10]; Cu-BTC at 1 bar (Cu). [11]

Their results show that the highest selectivity of CO_2 is 3.55 when $P=7.0$ MPa and $y_{\text{CO}_2}=0.2$.

Other groups evaluated the selectivity at low temperatures, finding extremely high values. For instance, Gatica et al. [3], reported a numerical study of adsorption of CO_2/CH_4 on carbon nanohorns, finding selectivities growing from 6 to 25 for a temperature drop from 193 K to 143 K. Maiga et al. [7,6], estimated the selectivity of a CO_2/CH_4 binary mixture in MOFs and graphene using GCMC and the ideal adsorbed solution theory (IAST). For MOFs, they predicted that the selectivity increased from 2 to 250 for temperatures dropping from 300 K to 120 K. For graphene at 40 K, the selectivity estimated by GCMC-IAST reaches the extremely high value of 6.24×10^6 . [6]

For practical reasons, it is vital to optimizing substrates capable of separation by adsorption at room temperature. In Fig. 1, we summarize the values of selectivities near 300 K reported by many groups.

We propose a simple substrate to reach high selectivity; it consists of graphene NRs placed over graphite. The NRs are assembled parallel to each other and the graphite surface. By tuning the separation between them, the edge style, and the distance between the NRs and graphite, we reach our objective.

Graphene NRs are quasi-one-dimensional carbon structures that can be obtained by cutting a graphene sheet

into strips of a few nanometers width [13]. Graphene is itself a unique material with a high specific surface area of $\sim 2600 \text{ m}^2/\text{g}$, which is obtained from graphite through oxidation, exfoliation, and reduction [14]. Ever since the experimental isolation of graphene in 2004, significant research efforts have been focused on investigating the electronic and transport properties of its NRs. Several techniques have been developed to fabricate them. These include electron beam lithography and etching, chemical synthesis, and unzipping of carbon nanotubes [15]. The properties of graphene nanoribbons can be tuned from metallic to semiconducting through changing the widths and the edge styles [16]. Paulla et al. [17] investigated graphene NRs for the sensing of carbon oxides. In their *ab initio* study, they found that pristine NRs may not be suitable for electrochemical sensing of carbon oxides with low concentration at room temperature; they suggest that adding an electric field can generate detectable coverages.

Although, in this work we do not address the technical aspects of keeping the graphene NRs fixed in place, we estimate that this can be accomplished by inserting spacers in between the NRs and the graphite surface, resembling the structure of MOFs or pillared graphene [18].

2 Methods

In this work, we compute, by MD simulations, the adsorption of a vapor mixture of CO_2 and CH_4 on the NRs/graphite substrate. We represent CH_4 as a neutral spherical molecule with zero electric dipole and quadrupole moments. The CH_4 - CH_4 intermolecular interaction energy is modeled as a Lennard Jones (LJ) potential. The LJ potential is given by,

$$U_{LJ} = 4\epsilon \left[\left(\frac{\sigma}{r} \right)^{12} - \left(\frac{\sigma}{r} \right)^6 \right], \quad (2)$$

where ϵ and σ are the energy and size LJ parameters, respectively, and r is the distance between atoms. The LJ parameters for CH_4 are $\epsilon = 148.0 \text{ K}$ and $\sigma = 3.7 \text{ \AA}$ adopted from Ref. [2]. We describe the CO_2 molecule as a linear rigid body with three LJ sites and three partial charges placed on each atom. The carbon atom has a positive charge $q_C = 0.576e$, and the oxygen atoms have a negative charge $q_O = -0.288e$. The bond length is $b = 1.18 \text{ \AA}$ [2]. The CO_2 - CO_2 intermolecular interaction energy is computed as a combination of the LJ and Coulomb potentials between partial charges. We adopt the LJ parameters from Ref. [2] (see table 1).

For different species, the cross parameters are calculated by using the Lorentz-Bertholet combination rules [19],

$$\sigma_{ij} = \frac{\sigma_{ii} + \sigma_{jj}}{2} \quad (3)$$

Table 1 Lennard Jones Parameters and Partial Charges.

Adsorbate	$\epsilon(\text{K})$	$\sigma(\text{\AA})$	$q(e)$
CH_4	148.0	3.7	0
C in CO_2	29.70	2.8	+0.576
O in CO_2	83.00	3.0	-0.288
C in Graphene	28.00	3.4	0

$$\epsilon_{ij} = \sqrt{\epsilon_{ii}\epsilon_{jj}} \quad (4)$$

In our simulations, we treat graphite as a continuous matter. The interaction energy between an adsorbate atom and the graphite substrate is evaluated by the Steele-10-4-3 potential [20] given by,

$$U_{\text{Steele}}(z) = 2\pi\epsilon\rho\sigma^2\Delta \left[\frac{2}{5} \left(\frac{\sigma}{z} \right)^{10} - \left(\frac{\sigma}{z} \right)^4 - \frac{\sigma^4}{3\Delta(z + 0.61\Delta)^3} \right], \quad (5)$$

where ϵ and σ are the LJ parameters and z is the distance between the adatom and the graphite surface; the number of carbon atoms per unit volume in graphite is $\rho = 0.114 \text{ \AA}^{-3}$, and the separation distance between the layers of graphitic carbon is $\Delta = 3.35 \text{ \AA}$.

We describe the interaction between the NRs and the adsorbates by a sum of LJ potentials. The NRs are kept rigid and fixed during the simulations.

We run MD simulations at constant temperature by using the Nose-Hoover thermostat, which is based on the extended Lagrangian method. We run our simulations with the LAMMPS program, which stands for (Large-scale Atomic/ Molecular Massively Parallel Simulator). [21, 22].

We set the simulation box with 160 \AA side lengths and periodic boundaries in XY directions. The box contains the right and left halves of two nanoribbons. The NRs are approximately 15-nm wide and infinitely long due to the periodic boundary conditions (see Fig. 2). The top wall of the box is reflective, and the graphite surface is at the bottom of the cell. To create the NRs we place a graphene layer above the graphite substrate and delete the carbon atoms within a selected narrow region. By cutting the graphene layer in the Y direction, we obtain zigzag NRs (ZRs), whereas cutting the graphene layer in the X direction, gives armchair NRs (ARs). By manipulating the region where the carbon atoms are deleted, we get two different styles of edges, as shown in Fig. 3. The figure represents the ZRs in the upper row and ARs in the lower row with two different edge styles: VV and VB. In style VV, the vertexes are facing vertexes, and the bays are facing bays. For style VB where the vertexes are facing the bays, the gap opening is characterized by parameter a . For style

VV, there are two parameters: b and c , which are the distance from bay to bay and vertex to vertex, respectively. To fine-tune the gap separation, we translate the NRs horizontally by tenths of angstroms.

The simulations are composed of two stages. First, we run a 1-million-steps MD of 50 CO_2 and 50 CH_4 molecules in the plain simulation box, to achieve a mixed vapor in equilibrium at 300 K. In the second stage, we include the graphite substrate and the NRs in the simulation box and run MD for 5 million fs-timesteps. Molecules are attracted to graphene and pass through the slit forming layers on the graphite surface and the bottom of the ribbons.

The usual definition of selectivity given in Eq. 1 assumes that the system is in equilibrium with a vapor. That is not the case in MD simulations, where the process described is rather dynamic. Some molecules leave the vapor to occupy the region next to the substrate, while the total number of molecules in the box remains constant. Depending on the amount adsorbed, the molecules remaining in the vapor phase are only a few or even zero. For this reason, we redefine the selectivity as

$$S = \frac{x_{\text{CO}_2}/x_{\text{CH}_4}}{y_{\text{CO}_2}/y_{\text{CH}_4}} \quad (6)$$

where x_i is the concentration of species i in the adsorbed phase, and y_i is the concentration in the simulation box. We compute x_i by counting the number of molecules in a region of thickness 5-Å above the graphite surface. To calculate the selectivity, we use the average of x_{CO_2} and x_{CH_4} over the last million steps (last nanosecond).

To assess the kinetics of the process we define the relative rate of adsorption R as,

$$R = \frac{r_{\text{CO}_2}}{r_{\text{CH}_4}}, \quad (7)$$

where r_{CO_2} and r_{CH_4} are the initial rate of adsorption for CO_2 and CH_4 , respectively. The rates r_i are calculated by a linear fit of the fraction adsorbed vs. time on the first nanosecond.

3 Results

We studied various combinations of gap openings, NRs-graphite distances (from 6 Å to 14 Å), and edge-styles (zigzag and armchair, VV and VB). In Table 2, we present the values of the selectivity and relative rate of adsorption for selected NRs with $S > 2$ or $R > 2$. In the cases where the adsorption of CH_4 is zero during the first nanosecond interval, we report $R \rightarrow \infty$. Also,

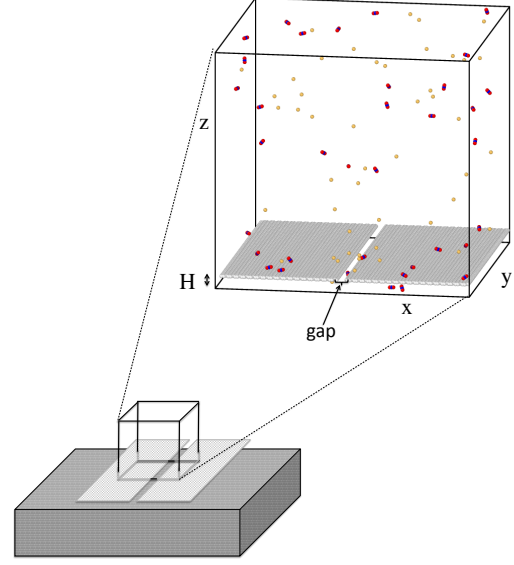


Fig. 2 Schematic picture of the nanoribbons over graphite and zoom of the simulation box.

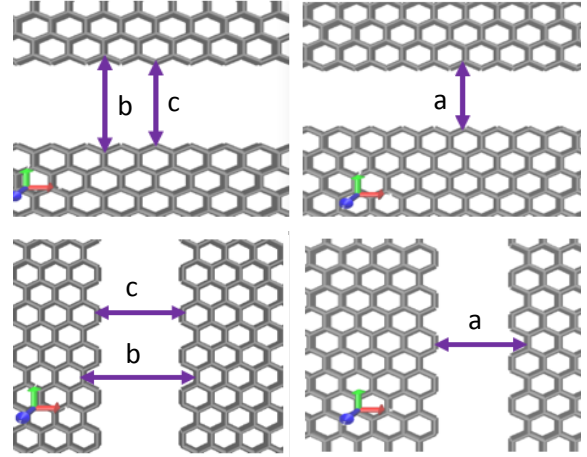


Fig. 3 Illustration of the edges of the graphene nanoribbons with styles zigzag-VV (top left), zigzag-VB (top right), armchair-VV (bottom left), armchair-VB (bottom right).

in the case of $x_{\text{CH}_4} = 0$ during the last nanosecond interval, the selectivity is infinite.

In Fig. 4 we show the results for the top-four selectivities. In the figure, we plot the adsorption of CO_2 and CH_4 on the graphite surface as a function of time. In the four cases, the graphene NRs are located at a distance $H = 6$ Å above graphite. The maximum selectivity was obtained for VB-edged ARs, with a vertex-bay distance of 7.4 Å (see Fig. 4, top left). In this case, CH_4 is wholly blocked out giving $S \rightarrow \infty$, and also due to zero CH_4 -adsorption in the first nanosecond, we obtain $R \rightarrow \infty$. The second top value of selectivity is 22 (Fig. 4 top right), for VV-edged ARs with parameters $b =$

9.8 Å and $c = 7.4$ Å; the value of R is 2.7. The third top value of selectivity is 21, shown in Fig 4 (bottom left). This case corresponds to VV-ARs with parameters $b = 14.8$ Å and $c = 12.3$ Å. The fourth top value is $S = 15$, achieved with VB-ZRs with parameter $a = 12.4$ Å. The last two cases also have high values of R (14 and 18).

In all cases with $H = 6$ Å methane does not fit in the space between the NRs and graphite. However, for wider gaps (second, third, and fourth cases), methane molecules are adsorbed on graphite at the slit opening. To exemplify, we show snapshots of the simulation cell at $t = 6$ ns in Figs. 5 and 6. Both cases correspond to $H = 6$ Å with gaps 7.4 Å (Fig. 5) and 14.8 Å (Fig. 6). For the 14.8-Å gap, we see in Fig. 6, a few CH_4 molecules adsorbed on graphite right at the slit.

As a reference for comparison, we simulated adsorption of the mixture on plain graphite, obtaining $S = 1.68$ and $R = 1.98$. As it results, the selectivity and R achieved with both ZRs and ARs are much higher than plain graphite.

When the distance between the graphene and graphite is higher than 8 Å and the gap opening wider than 6.9 Å in ZRs or 7.4 Å on ARs, the values of S and R are not better than plain graphite. On the other hand, any smaller gap opening yields zero adsorption, because the slit then becomes too narrow for any molecule to pass. A distance $H < 6$ Å results in zero adsorption as well, because the NRs-graphite separation becomes too thin to allow any of the molecules within.

The structure of the molecules play a crucial role; only the linear CO_2 fits in the 6-Å narrow space between the NRs and graphite while the spherical CH_4 does not. Moreover, the Van der Waals interaction between CO_2 and graphite is stronger than CH_4 -graphite. In our simulations, we computed the average adsorption energy between graphite and CO_2 , $E_{G-\text{CO}_2} = 3.76$ Kcal/mol, while $E_{G-\text{CH}_4} = 2.64$ Kcal/mol. As a result, the selectivity for CO_2 is high due to a combination of energetic and steric effects.

The kinetics of adsorption is also greatly improved. In plain graphite, the initial uptake of CO_2 is just twice as fast as for CH_4 . In the NRs/graphite substrate, the relative rate R reaches 18 and 14 for ZRs and ARs, respectively.

4 Discussion

Our findings show that the separation of a carbon dioxide and methane mixture on NRs-Graphite at room temperature is significantly enhanced. All the NRs edges tested in this work are adequate for filtering carbon dioxide.

The mechanisms involved in the performance of the filter combine energetics, kinetics, and steric aspects of adsorption. The energetics works because CO_2 is more intensively attracted to the substrate; the kinetic factor arises from the higher initial rate of adsorption of CO_2 even in non-blocking cases. There is an interplay of adsorption and diffusion above and below the graphene NRs and on graphite. CO_2 adsorbs first on top of the graphene, followed by CH_4 . Then, CO_2 diffuses through the gap and forms monolayer films on the graphite surface and below the NRs. If the distance between the NRs and graphite is 6 Å, CH_4 is completely blocked out even with wide enough NRs gap openings. This is a consequence of the overlap of the repulsive cores of the CH_4 -graphene and CH_4 -graphite interactions that results in a total repulsion of methane. In the non-blocking cases, CH_4 molecules would start adsorbing on graphite later than CO_2 .

The optimal parameters for the filter are a NRs-graphite separation of 6 Å, armchair-VB edge style, and gap opening of 7.4 Å. However, slightly larger separations and openings and other edge styles are also effective.

As mentioned above, although we have not addressed the technical aspects of keeping the graphene NRs fixed in place, we would estimate that this can be accomplished by inserting organic molecules as pillars resembling the structure of pillared graphene [18]. However, the optimal separation of 6 Å may be too small to be achieved by a pillared structure. In this case, we would envision a different approach similar to the graphite intercalation compounds [23]. Of course, the technicality is far from the scope of our work. However we must say that adding such pillars or spacers would affect the adsorption rates but not the fact that methane is blocked out when the separation is 6 Å wide. Finally, the reader may argue that the proposed substrate lacks the capacity for storage. That is true, and we would like to emphasize that our results pertain to the filtering rather than the storage. As such, the filter should be combined with a supplementary substrate for that purpose.

Acknowledgements This work used the Extreme Science and Engineering Discovery Environment (XSEDE) through allocation TG-DMR180036.

Conflict of interest

The authors declare that they have no conflict of interest.

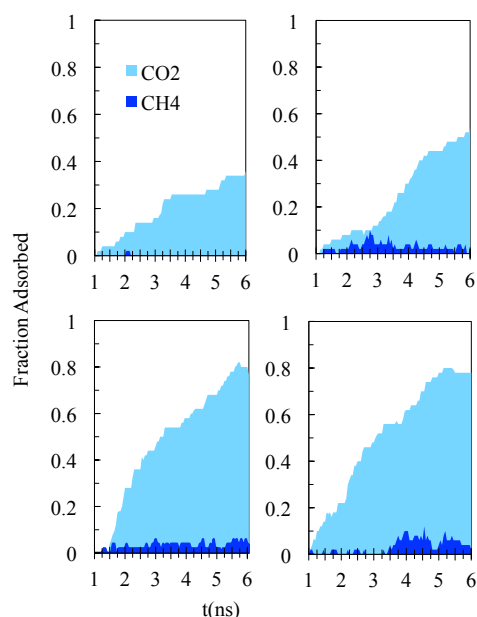


Fig. 4 Fraction adsorbed on graphite x_{CO_2} (lightblue) and x_{CH_4} (blue) on the graphite surface. The graphene ribbons are placed at a distance $H = 6$ Å above the graphite. The edge styles are armchair VB with parameter $a = 7.4$ Å (top left), armchair VV with $b = 9.8$ Å and $c = 7.4$ Å (top right), armchair VV with $b = 14.8$ Å and $c = 12.3$ Å (bottom left) and zigzag VB with $a = 12.4$ Å (bottom right).

Table 2 Selectivity and relative rate of adsorption for selected slit openings.

H(Å)	Style	Gap(Å)	S	R
6	A VB	7.4	∞	∞
6	A VV	9.8	22	2.7
6	A VV	14.8	21	14
6	Z VB	12.4	15	18
6	Z VV	14.2	11	9.6
6	Z VB	6.9	8.8	12
12	A VB	7.4	8.6	4.0
12	Z VB	6.9	8.4	14
6	A VV	12.3	7.9	11
10	A VB	7.4	7.5	8.5
14	A VB	7.4	7.0	4.3
6	Z VV	9.8	6.5	6.9
10	Z VB	6.9	6.5	2.7
14	Z VB	6.9	6.1	∞
8	Z VB	6.9	5.9	2.7
8	A VB	7.4	5.5	3.8
14	Z VB	12.4	1.9	3.1
14	Z VV	9.8	1.8	3.3

References

1. I. Bastin, P.S. Barcia, E.J. Hurtado, J.A.C. Silva, A.E. Rodrigues, B. Chen, The J. of Phys. Chem. C **112**, 1575

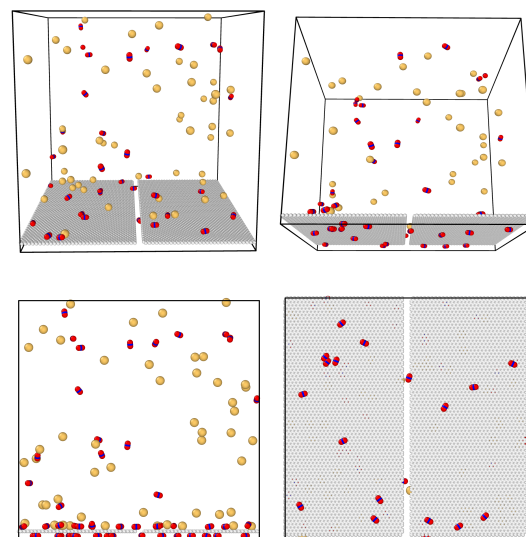


Fig. 5 Snapshots of the simulation at $t = 6$ ns, showing CH_4 in yellow and CO_2 in blue-red. The molecules are not in scale. The graphite surface is not shown for clarity. The panels display two perspective views (top row), a side view (bottom left) and a view from below the NRs (bottom right). The NRs' edges are armchair-VB with a 7.4-Å gap, and $H = 6$ Å.

- (2008)
2. R. Babarao, Z. Hu, J. Jiang, Langmuir **23**, 659 (2007)
3. S.M. Gatica, A. Nekhai, A. Scrivener, Molecules **21** (2016)
4. M. Heuchel, G.M. Davies, E. Buss, N.A. Seaton, Langmuir **15**, 8695 (1999)
5. Y. Liu, J. Wilcox, Environmental Science and Technology **47**, 95 (2013)
6. S.M. Maiga, PhD. Dissertation, Howard University Washington, D.C (2016)
7. S.M. Maiga, M.A. Medina, O.J. Durodola, S.M. Gatica, J. of Low Temperature Phys. **172**, 274 (2013)
8. J.C. Palmer, J.D. Moore, T.J. Roussel, J.K. Brennan, K.E. Gubbins, Phys. Chem. Chem. Phys. **13**, 3985 (2011)
9. X. Peng, D. Cao, J. Zhao, Separation and Purification Technology **68**, 50 (2009)
10. Y. Chen, D. Lv, J. Wu, J. Xiao, H. Xi, Q. Xia, Z. Li, Chemical Engineering Journal **308**, 1065 (2017). DOI <https://doi.org/10.1016/j.cej.2016.09.138>. URL <http://www.sciencedirect.com/science/article/pii/S1385894716313833>
11. B. Szcześniak, J. Choma, Microporous and Mesoporous Materials **292**, 109761 (2020). DOI <https://doi.org/10.1016/j.micromeso.2019.109761>. URL <http://www.sciencedirect.com/science/article/pii/S1387181119306183>

23. M.S. Dresselhaus, G. Dresselhaus, *Advances in Physics* **30**(2), 139 (1981). DOI 10.1080/00018738100101367

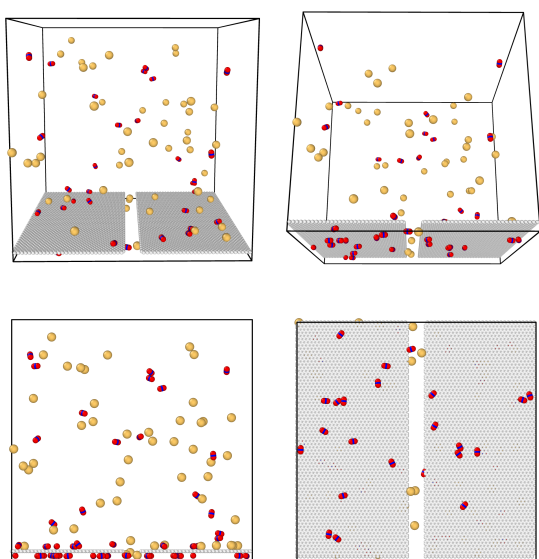


Fig. 6 Snapshots of the simulation at $t = 6$ ns, showing CH_4 in yellow and CO_2 in blue-red. The molecules are not in scale. The graphite surface is not shown for clarity. The panels display two perspective views (top row), a side view (bottom left) and a view from below the NRs (bottom right). The NRs' edges are armchair-VV with a $14.8\text{-}\text{\AA}$ gap, and $H = 6\text{ \AA}$.

12. M. Wang, Z. Zhang, Y. Gong, S. Zhou, J. Wang, Z. Wang, S. Wei, W. Guo, X. Lu, *Applied Surface Science* **502**, 144067 (2020). DOI <https://doi.org/10.1016/j.apsusc.2019.144067>. URL <http://www.sciencedirect.com/science/article/pii/S0169433219328831>
13. V.A. Soroko, K.G. Batrakov, L.A. Chirnozatskii, *Phys. of the Solid State* **56**, 2135 (2014)
14. S. Gadipelli, Z. Xiao Guo, *Progress in Materials Science* **69**, 1 (2014)
15. A. Orlof, J. Ruseckas, I.V. Zozoulenko, *Phys. Rev. B* **88**, 125409 (2013)
16. W. Yin, Y. Xie, L. Liu, Y. Chen, R. Wang, X. Wei, J. Zhong, L. Lau, *J. of Applied Phys.* **113**, 173506 (2013)
17. K.K. Paulla, A.A. Farajian, *The Journal of Physical Chemistry C* **117**(24), 12815 (2013). DOI 10.1021/jp312711s. URL <https://doi.org/10.1021/jp312711s>
18. G.K.D.E. Tylanakis, G.E. Froudakis, *Nano Letters* **8**(10), 3166 (2008). DOI 10.1021/nl801417w. URL <https://doi.org/10.1021/nl801417w>. PMID: 18800853
19. L.W. Bruch, M.W. Cole, E. Zaremba, *Physical Adsorption: Forces and Phenomena* (Clarendon Press, Oxford, 1997)
20. W. A. Steele, *Surface Science* **36**, 317 (1973). DOI 10.1016/0039-6028(73)90264-1
21. S. Plimpton, *J. of Computational Phys.* **117**, 1 (1995)
22. LAMMPS website. <http://lammmps.sandia.gov>. [Accessed: 10-August 2019]